Emergent Mechanics of Magnetic Skyrmions Deformed by Defects

Linjie Liu,[1,2,3] Weijin Chen,[1,2,3,4,*] and Yue Zheng[1,2,3,†]
[1]Guangdong Provincial Key Laboratory of Magnetoelectric Physics and Devices, School of Physics, Sun Yat-sen University, Guangzhou 510275, China
[2]State Key Laboratory of Optoelectronic Materials and Technologies, School of Physics, Sun Yat-sen University, 510275 Guangzhou, China
[3]Centre for Physical Mechanics and Biophysics, School of Physics, Sun Yat-sen University, 510275, Guangzhou, China
[4]School of Materials, Sun Yat-sen University, 518107 Shenzhen, China

(Received 21 July 2023; revised 20 October 2023; accepted 21 November 2023; published 12 December 2023)

While magnetic skyrmions are often modeled as rigid particles, both experiments and micromagnetic simulations indicate their easy-to-deform characteristic, especially when their motion is restricted by defects. Here we establish a theoretical framework for the dynamics of magnetic skyrmions by incorporating the degrees of freedom related to deformation and predict well the current-driven dynamics of deformable skyrmions in the presence of line defects without any parameter fitting, where classical theories based on rigid-particle assumption deviate significantly. Further, we define an emergent property of magnetic skyrmions—*flexibility* and show that this property strongly modulates the depinning dynamics of skyrmions along a line defect with breaches. Our work explores the emergent mechanics of magnetic skyrmions and extends the current understanding on the dynamics of skyrmions interacted with defects.

DOI: 10.1103/PhysRevLett.131.246701

Magnetic skyrmions are a class of swirling spin textures with an integral topological charge [1–3]. Because of their small sizes, intriguing physical properties [4], and characteristics in response to external stimuli like electric current [5,6] or magnetic field [7,8], magnetic skyrmions are considered as promising candidates in next-generation spintronic devices [9,10]. Since the first experimental report around 2009 [11], magnetic skyrmions have attracted considerable attention, particularly on their current-driven dynamics, with various device concepts being proposed.

Magnetic skyrmions are usually treated as rigid particles in theoretical studies [12,13], and their transport behaviors are analytically described by the classical Thiele's equation [14]. This theory has achieved great success in describing the motion of magnetic skyrmions, particularly providing an intuitive explanation of the skyrmion Hall effect [15,16] by deriving a topology-related Magnus force in the motion equation. However, this first version of emergent mechanic framework for the motion of magnetic skyrmions neglects any possible deformation, which is commonly observed in both simulations and experiments [17–19] and is noticeable even under small currents [20]. Importantly, defects in real samples (e.g., natural edges, grain boundaries, impurities, etc.) would cause more severe deformation of skyrmions by restricting their motion [21–23]. Deformation of skyrmions significantly affects their motion dynamics that is crucial to their applications, e.g., it brings large inertias [24] and can even lead to topology-irrelevant skyrmion Hall effect [25,26]. The deformability of skyrmions also makes them promising in new frontiers like reservoir computing [27] and random number generation [23]. However, a mechanical framework for the dynamics (i.e., deformation and motion, and their interplay) of magnetic skyrmions has not yet been established.

Over the years, the interplay of deformation and motion has been an important issue of the dynamics of magnetic textures. For magnetic domain walls or vortexes, well-known concepts such as linear mobility [28], Döring mass [29], Walker breakdown [30], and oscillatory behavior [31,32] have been established. In a microscopic view, the motion and deformation of magnetic textures are collective modes of spins. Therefore, both these behaviors can be formulated by using a unified series of collective coordinates $\boldsymbol{\xi}(t) = \{\xi_0, \xi_1, \xi_2, \ldots\}$. In principle, the number of collective modes of a magnetic texture is infinite, but its motion and deformation behaviors are mainly determined by a couple of soft modes with long relaxation times [31–36]. To capture the dynamics of magnetic skyrmion, it is crucial to find those soft modes related to not only motion but also deformation and explore the interaction of these modes.

In this Letter, we establish a theoretical framework for the dynamics of magnetic skyrmions by incorporating two geometry-related coordinates, radius R and wall width w, into the classical Thiele' equation. The balance equation in terms of the new coordinates R and w and the generalized forces are derived. Based on this framework,

the current-driven dynamics of deformable skyrmions in the presence of line defects can be predicted without parameters fitting. Interestingly, as an emergent behavior, the deformation of skyrmions violates conventional elastic mechanics such as the Saint-Venant's principle and positive Poisson's ratio. Furtherly, we quantify the deformability of skyrmions by introducing an emergent property, *flexibility* of skyrmions. Flexibility is demonstrated to strongly modulate the depinning dynamics of the skyrmion moving along a line defect with breaches, implying a potential skyrmion valve.

We consider a Néel-type skyrmion system consisting of a ferromagnetic (FM) layer and a heavy-metal (HM) layer. The Hamiltonian $\mathcal{H}$ of the system is expressed as [37,38]

$$\mathcal{H} = \int \Big\{ A(\nabla \boldsymbol{m})^2 + D\big[m_z(\nabla \cdot \boldsymbol{m}) - \boldsymbol{m} \cdot \nabla m_z\big] - Km_z^2 - \frac{1}{2}\mu_0 \boldsymbol{H}_\mathrm{d} \cdot \boldsymbol{m} \Big\} \mathrm{d}V. \quad (1)$$

Here, $\boldsymbol{m}$ denotes the unit vector of magnetization field; m_z is its z component; A, D, and K are the Dzyaloshinskii-Moriya interaction (DMI) constant [37,38], perpendicular magnetic anisotropy (PMA), and magnetostatic field, respectively. $\boldsymbol{H}_\mathrm{d}$ is the exchange stiffness.

The dynamics of magnetization field $\boldsymbol{m}$ is governed by the Landau-Lifshitz-Gilbert (LLG) equation,

$$\dot{\boldsymbol{m}} = -|\gamma| \boldsymbol{m} \times \boldsymbol{H}_\mathrm{eff} + \alpha(\boldsymbol{m} \times \dot{\boldsymbol{m}}) + \tau_\mathrm{SOT}, \quad (2)$$

where γ and α are the gyromagnetic ratio and Gilbert damping parameter, respectively. $\boldsymbol{H}_\mathrm{eff}$ is the effective field, which is expressed as $\boldsymbol{H}_\mathrm{eff} = -\delta\mathcal{H}/\delta\boldsymbol{m}$. τ_SOT represents a dampinglike spin-orbit torque (SOT).

With the collective coordinates are $\boldsymbol{\xi}(t) = \{\xi_0, \xi_1, \xi_2, \ldots\}$, the deformation of magnetic textures can be interpreted as the generalized displacement along the ξ_i axis. The magnetization field can then be expressed as $\boldsymbol{m}(t) = \boldsymbol{m}[\boldsymbol{r}, \boldsymbol{\xi}(t)]$. Thus, the generalized dynamic equation of magnetic structures can be directly derived from the LLG equation (see derivation details in the Supplemental Material [39]),

$$F_{\xi_i}^G - F_{\xi_i}^D = F_{\xi_i}^{\mathcal{H}} + F_{\xi_i}^{\mathrm{SOT}}. \quad (3)$$

Here, the ξ_i component of the jth generalized force $F_{\xi_i}^j$ is expressed as $F_{\xi_i}^j = -\int (\boldsymbol{m} \times \boldsymbol{L}^j) \cdot \partial \boldsymbol{m}/\partial \xi_i \mathrm{d}V$, where the $\boldsymbol{L}^j$ is the jth term of the LLG equation. When the deformation of the skyrmion is neglected, only translation modes are involved. The collective coordinates are chosen as $\xi_i = X, Y$, where X and Y are coordinates of the skyrmion center. Equation (3) then reduces to the classical Thiele's equation,

$$4\pi Q \hat{\boldsymbol{e}}_z \times \boldsymbol{v} - \Gamma \boldsymbol{v} = \beta_\mathrm{H} \Lambda \boldsymbol{J} + \nabla \varphi_\mathrm{sk}, \quad (4)$$

where Q is topological charge, $\boldsymbol{v}$ is the velocity of the skyrmion, $\boldsymbol{J}$ is the current density, φ_sk is the potential of the skyrmion, β_H is the SOT parameter, Λ is the driving factor, and Γ is the damping factor.

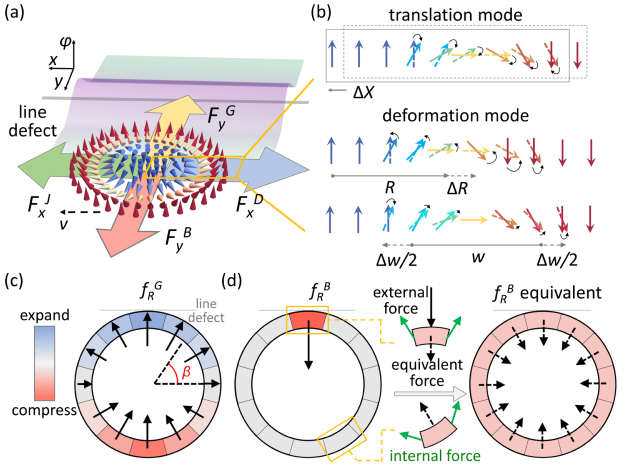

FIG. 1. Schematic illustration of the generalized dynamic model of a deformable magnetic skyrmion interacted with a line defect. (a) Force balance diagram. (b) Translation and deformation modes of a skyrmion texture. (c) Effect of the generalized gyrotropic force on different segments of the skyrmion wall. The inward and outward arrows represent compression and expansion, respectively. (d) Effect of the generalized blocking force on different segments of the skyrmion wall. Green arrow and dashed arrow represent the internal forces and equivalent joint force, respectively.

We apply this theoretical framework to the dynamics of the skyrmion in the presence of a line defect. Line defects are quite common in racetrack-type structures, which can be natural edges or defect tracks with different magnetic interactions from the bulk region [26]. In this work, four types of line defects (either with higher PMA, higher exchange stiffness, or lower DMI than the bulk region, or are natural truncated edges) are studied, and they impose an energy barrier to the skyrmion. In our model system, both the line defect and the applied current are set to be along the x axis [Fig. 1(a)]. Along the y axis, the skyrmion experiences two forces, the gyrotropic force $F_y^G = 4\pi Q v$ and the blocking force by the line defect $F_y^B = \partial \varphi_{sk}/\partial y$.

To establish the equilibrium equation of the generalized forces in terms of the generalized coordinates, we express the magnetization of the skyrmion in an analytical way as $\boldsymbol{m} = (\sin\theta\cos\phi, \sin\theta\sin\phi, \cos\theta)$ [40]. Here, horizontal angle θ satisfies $\theta = 2\arctan[\sinh(r/w)/\sinh(R/w)]$; azimuthal angle ϕ is expressed as $\phi = \beta + \psi$; β and r are the polar angle and polar radius in polar coordinates; R, w, and ψ are the radius, wall width, and precession angle of the skyrmion (see Fig. S2 [39]). Among the various modes of deformation, radially symmetric modes of the radius $\xi_1 = R$ and the wall width $\xi_2 = w$ [Fig. 1(b)] are the primary deformation modes [39]. Other modes like the precession angle, the angle variation of the radius, and the wall width are hard modes and their contributions to

skyrmion dynamics can be ignored. In this case, R and w are irrelevant with β and $\psi = 0$. Then, the equilibrium equations of the generalized forces are only functions of R and w. By substituting $\boldsymbol{m}$ into the LLG equation [Eq. (2)], we can derive the equilibrium equations of the generalized forces as functions of R and w (see Supplemental Material, Sec. S3 [39] for details).

Note that not all the terms in the LLG equation [Eq. (2)] are relevant to the deformation of the skyrmion. For example, the gyrotropic term, which leads to the first term in Eqs. (3) and (4), contributes to a generalized gyrotropic force F_R^G acting on coordinate R, with $F_R^G = \int f_R^G \mathrm{d}\beta = -\int 2v \sin\beta \mathrm{d}\beta$. Here, $f_R^G(\beta)$ is the generalized gyrotropic force distributed on each segment of skyrmion wall in polar angle β. As shown in Fig. 1(c), the effect of gyrotropic force on each segment mutually cancels. Overall, it does not affect the radius of skyrmion and $F_R^G = 0$. Similarly, the SOT term is also zero. Moreover, for steady deformation, $\dot{R} = \dot{w} = 0$, and the generalized damping forces satisfy $F_R^D = F_w^D = 0$.

Only the conservative terms related to $\mathcal{H}$ expressed as $F_i^j = \gamma \int \delta\mathcal{H}_j/\delta\xi_i \mathrm{d}V$ contribute to the deformation of skyrmion, where the total Hamiltonian $\mathcal{H} = \mathcal{H}_\mathrm{S} + \mathcal{H}_\mathrm{B}$ is contributed by the magnetic interaction of the system $\mathcal{H}_\mathrm{S}$ and the energy barrier of defects $\mathcal{H}_\mathrm{B}$. $\mathcal{H}_\mathrm{S}$ has the same form as the pristine system but the form of $\mathcal{H}_\mathrm{B}$ is still unknown. The equilibrium equations of generalized forces in Eq. (3) are reduced to $F_R^\mathrm{S} - F_R^\mathrm{B} = 0$ and $F_w^\mathrm{S} - F_w^\mathrm{B} = 0$.

When the skyrmion approaches the defect, only a small part of skyrmion enters the defect region. In this case, energy increases solely in the segment of the skyrmion nearest to the defects [the upper-most segment in Fig. 1(d)]. This effect prevents skyrmion furtherly entering the defect region. Meanwhile, the increasing energy leads to a strong compressive force exerted on the segments closest to the defect [as shown in Fig. 1(d)]. To maintain the circular shape of skyrmion, the nearby segments generate internal forces to counterbalance the external force. Ultimately, the external force exerted on local segment of skyrmion is evenly distributed throughout the entire skyrmion and results in an overall compression. In this case, the energy penalty due to entering the defect region by dy is equal to that caused by skyrmion expansion by δR, i.e., $\int \delta\mathcal{H}_\mathrm{B}/\delta R \mathrm{d}V = \partial\varphi/\partial Y$ [39]. Moreover, according to Thiele's equation [Eq. (4)], $\partial\varphi/\partial Y = 4\pi Q v$. In this way, we acquire the value of F_R^B without knowing the specific form of $\mathcal{H}_\mathrm{B}$. Similarly, we can demonstrate that $F_w^\mathrm{B} = 0$, and Eq. (3) can be expressed as

$$\int \gamma \frac{\delta\mathcal{H}_\mathrm{S}}{\delta R} dV + 4\pi Q v = 0,$$
$$\int \frac{\delta\mathcal{H}_\mathrm{S}}{\delta w} dV = 0. \tag{5}$$

Based on this approach, the deformation denoted by radius R and wall width w of skyrmions under external currents can be solved directly without any parameter fitting.

We emphasize the nature of skyrmion deformation as an emerging mechanics phenomenon. That is, we can establish balanced equations for the deformation mode coordinates, as what has been done by the classical Thiele's theory for the translation mode of skyrmion. Here, we show that both the deformation and translation modes are associated with specific spin-flipping processes, and their generated virtual works are interconnected. Thus, a relationship between the generalized forces of these modes can be established. The interaction between the skyrmion and defects is commonly considered to be a complex problem, as it is challenging to determine how defects affect the local interaction of spins. However, by associating the motion and deformation of skyrmions in view of emergent mechanics, this problem is greatly simplified. Our conclusion is, *the deformation of the skyrmion is only related to its motion characteristics* (see Supplemental Material, Sec. S4 [39] for details).

To verify our model (hereafter we call it the flexible model in contrast to the classical rigid model), the dynamics of a series of skyrmions with similar size and mobility but with different flexibility (a quantitative definition will be given later) are simulated in the presence of a line defect. By varying PMA constant K and DMI constant D simultaneously, the radii and mobility of the skyrmions are controlled as ~13 nm and $\sim 6 \times 10^{-10}$ m^3/C [39]. The line defect is in 4 nm width (with the K_defect 1.5 times higher than that in the bulk region) and exerts a large enough energy barrier to block the skyrmion. Figure 2(a) shows the trajectories of a relatively soft skyrmion ($K = 1 \times 10^5$ J/m^3) and a relatively hard skyrmion ($K = 10 \times 10^5$ J/m^3) under the same current density

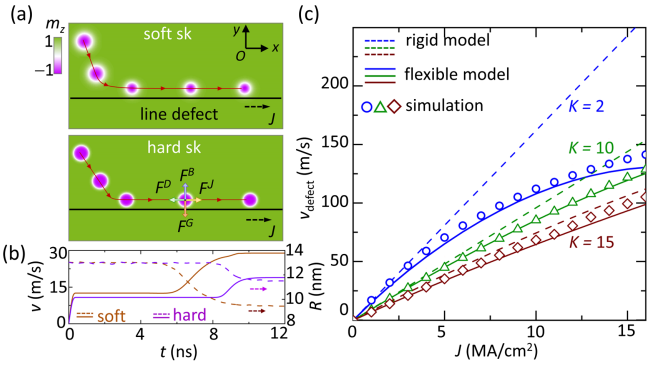

FIG. 2. Dynamics of skyrmions interacted with a line defect. The micromagnetic simulation results of (a) the trajectories and (b) the velocity and size variations of two skyrmions with similar size but different flexibility. (c) Comparison of the predicted skyrmion velocity by micromagnetic simulation, Thiele's model based on rigid particle assumption (rigid model), and our model including deformation of the skyrmion (flexible model).

($J = 2$ MA/cm^2). The velocity and size evolution curves of the two skyrmions are shown in Fig. 2(b). It is clear that the two skyrmions have similar sizes and velocities when they are far away from the line defect. However, when they approach the line defect, they exhibit different size changes and acceleration. The deformation and acceleration of the soft skyrmion are much larger than those of the hard one. Such an acceleration effect originates from the balance of the gyrotropic force and the defect blocking force [48,49]. The velocity of the skyrmion along the line defect is given by $v_{\mathrm{d}} = \beta_{\mathrm{H}} J\Lambda/\Gamma$, where Λ and Γ satisfy $\Lambda = \pi^2 R$ and $\Gamma = 2\pi\alpha(R/w + w/R)$ [41].

The deformation of the skyrmion is expressed in term of change in R and w as $\varepsilon_R = \Delta R/R_0$, $\varepsilon_w = \Delta w/w_0$, similar to elastic mechanics. R_0 and w_0 are the radius and wall width of skyrmions without deformation, where R_0 and w_0 satisfy $R_0 = \pi D\sqrt{A/(16AK^2 - \pi^2 D^2 K)}$ and $w_0 = \pi D/4K$ [40]. According to the second formula in Eq. (5), no external force is exerted on the general coordinate w. Thus, R and w need to satisfy a specific relation, $\varepsilon_w = -\kappa_{sk}\varepsilon_R$. Here, $\kappa_{sk} = -A/(A + KR^2)$ is defined as Poisson's ratio of the skyrmion, and it has a negative value. One can use ε_R to evaluate the skyrmion deformation. In this case, motion of the deformed skyrmion can be described by an extended Thiele equation,

$$4\pi Q\hat{\boldsymbol{e}}_z \times \boldsymbol{v} - \Gamma_0 \boldsymbol{v} = \beta_{\mathrm{H}}\Lambda_0 \boldsymbol{J} + \boldsymbol{F}^{\mathrm{deform}} + \nabla\varphi_{\mathrm{sk}}. \quad (6)$$

Here, $\boldsymbol{F}^{\mathrm{deform}} = -\Gamma_0(b_1\varepsilon_R - b_2\varepsilon_R^2)\boldsymbol{v} - \beta_H\Lambda_0\varepsilon_R\boldsymbol{J}$ is the additional deformation term. Γ_0 and Λ_0 are the damping and driving factors of skyrmion without deformation. b_1 and b_2 are geometry parameters given by $b_1 = (1 - \eta_R^2)^2/(1 + \eta_R^2)$ and $b_2 = 1.5\eta_R^2 b_1$, with $\eta_R = w_0/R_0$.

For the classical rigid model, the radius and wall width of the skyrmion are fixed and thus, the v-J curve exhibits linearity. For our model with the deformation of the skyrmion taken into account, the dependent between v_{d} and J is no longer linear. Based on Eqs. (5) and (6), v_{d} can be solved analytically. We compare the analytical results of these two models with the micromagnetic simulation results [Fig. 2(c)]. For hard skyrmions (K is large), both models work in a wide range of current density J. For soft skyrmions (K is small) at low J, as the deformation of the skyrmion is small, both models are still in good agreement with the simulation results. As J increases, however, the deformation of the skyrmion becomes nonnegligible and causes nonlinearity of the v-J curve. In this case, our flexible model that incorporates deformation of the skyrmion is still in good agreement with the simulation results, in contrast to the rigid model.

A critical question remains unclear: how to quantify the deformability of the skyrmion? To answer this question, we simulate the deformation of the skyrmion at different current densities. Meanwhile, based on Eq. (5) we can define the effective force of the skyrmion resisting external current as $F^{\mathrm{eff}} - J = 0$. The effective force can be expressed as $F^{\mathrm{eff}} = \gamma \int \delta\mathcal{H}_s/\delta R \mathrm{d}V(R^2 + w^2)/4\pi\beta' w R^2$. Retaining the first two orders about ε_R, the equilibrium equations of the first formula in Eq. (5) is rewritten as

$$\frac{1}{\lambda_1}\varepsilon_R + \frac{1}{\lambda_2}\varepsilon_R^2 - J = 0. \quad (7)$$

Here, λ_1 and λ_2 are the first and second order of flexibility. λ_1 and λ_2 satisfy $\lambda_1 = 8KR_0^2/\pi^2\gamma\beta' D^2$ and $\lambda_2 = \lambda_1/5$. Constant β' satisfies $\beta' = \pi\beta H/2\alpha$. Thus, we can define the flexibility of the skyrmion as λ_1, which quantifies the ability of the skyrmion to generate an effective force by inducing deformation. The skyrmion with higher flexibility requires larger deformation to generate equivalent forces resisting the external current.

The predicted ε_R and ε_w by micromagnetic simulation and the developed flexible model are shown in Figs. 3(a)

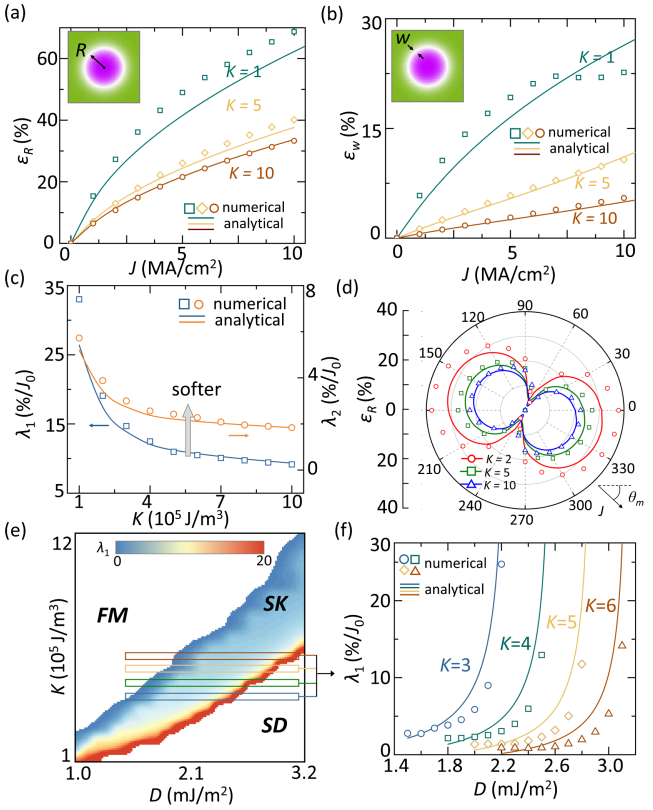

FIG. 3. Deformation of the skyrmion at different current densities. Dependence of (a) ε_R and (b) ε_w on current density. K is in unit of 10^5 J/m^3. (c) The predicted dependence of ε_R on the direction of applied current θ_m by the flexible model and simulation. (d) The predicted flexibility of skyrmions with similar size but different K by micromagnetic simulation and the analytical flexible model. J_0 is in units of MA/cm^2. (e) K-D phase diagram of skyrmion flexibility. FM, SK, and SD represent the ferromagnetic, skyrmion, and stripe-domain phases, respectively. (f) Comparison between the analytical and numerical results of flexibility of skyrmions under different PMA and DMI.

and 3(b). The results predicted by the flexible model and simulation are in good agreement. We further calculate the flexibilities of skyrmions with similar size as a function of perpendicular anisotropy K based on the micromagnetic simulation and our model [Fig. 3(c)]. In good consistence with simulation, our model shows that the flexibility of the skyrmion in similar size increases as K increases.

Moreover, our model can be generalized to any direction of the applied current and Eq. (7) is rewritten as

$$\int \gamma \frac{\delta \mathcal{H}_S}{\delta R} dV + 4\pi Q v \cos\theta_m + \beta_H \Lambda J \sin\theta_m = 0,$$
$$\int \frac{\delta \mathcal{H}_S}{\delta w} dV = 0. \quad (8)$$

Here, θ_m is the angle between the current and the line defect. The dependence of ε_R on θ_m for skyrmions with similar size but different K is further predicted by the flexible model and simulation [Fig. 3(d)]. Here, J is fixed at 5 MA/cm^2. The symmetry axes of the deformation curves are related to the Hall angle of the skyrmion. Further, we simulate the K-D phase diagram of skyrmion flexibility [Fig. 3(e)]. It is found that the flexibility of skyrmion λ_1 increases rapidly near the phase boundary between the skyrmion (SK) and stripe-domain (SD) phases, very much like the magnetic and dielectric permittivity of ferromagnetic and ferroelectric materials. This is because near the phase boundary, the energy of the skyrmion is close to the ferromagnetic background, and the energy penalty due to deformation is small. Comparison between numerical and analytical results is shown in Fig. 3(f). Again, the results are in good agreement with each other. We therefore establish an effective analytical model to predict the deformation of the skyrmion.

We finally show the effect of flexibility on the depinning characteristics of skyrmions. When interacting with defects, skyrmions can either directly penetrate through the defects or bypass the defects (i.e., through the gap between defects) [26]. Apparently, whether a skyrmion can bypass the defects is related to its size, the gaps between defects, as well as its flexibility. As the flexibility of the skyrmion becomes smaller, its deformation will be smaller, making it more difficult for it to "squeeze" through the defect gaps. The dynamics of skyrmions near a line defect with a breach is simulated and the results are shown in Fig. 4. These skyrmions have similar size but different flexibilites. The size of the breach is smaller than that of the skyrmion, requiring a specific threshold current density to enable the passage of skyrmion. It shows that the critical depinning current density varies 3 to 5 times due to the difference of flexibility, implying the important role of this emergent mechanic property playing in skyrmion dynamics.

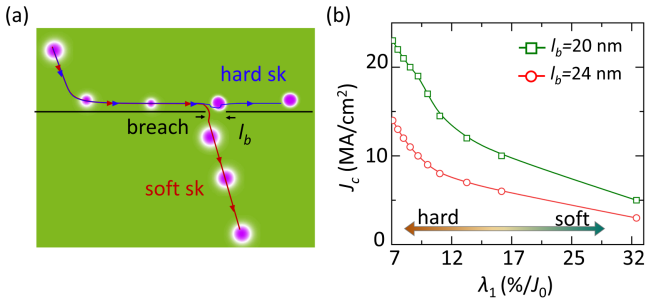

FIG. 4. The influence of flexibility on the dynamics of skyrmions near a line defect with a breach. (a) Trajectories of two skyrmions with similar size but different flexibility. (b) Dependence of the critical depinning current density on the flexibility of the skyrmion.

In conclusion, a theoretical framework for the dynamics of magnetic skyrmions is established by incorporating the deformation coordinates. Based on our model, the current-driven dynamics of deformable skyrmions in the presence of line defects can be analytically predicted and agrees well with the micromagnetic simulation, in contrast to the classical rigid-particle model. An emergent property of skyrmions—*flexibility* is defined and its important role in current-driven skyrmion dynamics is emphasized. Our work attempts to develop the emergent mechanics for the deformation and motion dynamics of magnetic skyrmions and extends our current understanding on the dynamics of skyrmions. Apart from the cases of line defects, flexibility also largely affects the transport characteristics of the skyrmion in the presence of point defects (see Supplemental Material, Sec. S7 [39] for details). Our model is also appliable to other nonlinear response of motion [50] or compression behavior of skyrmions [42,51,52]. The case of different type of defects like notch, point defect, and other deformation cases of skyrmions can also be handled in a similar way.

The authors thank helpful discussions from Professor H. Wen and Professor W. Zhu. The authors acknowledge support by Grants from National Natural Science Foundation of China (No. 12302211, No. 12222214, No. 11972382, and No. 12132020), Guangdong Provincial Key Laboratory of Magnetoelectric Physics and Devices (No. 2022B1212010008) and by the Shenzhen Science and Techonlogy Program (Grants No. 202206193000001, No. 20220818181805001).

*chenweijin@mail.sysu.edu.cn
†zhengy35@mail.sysu.edu.cn

[1] U. K. Roessler, A. Bogdanov, and C. Pfleiderer, Nature (London) **442**, 797 (2006).
[2] X. Z. Yu, Y. Onose, N. Kanazawa, J. H. Park, J. H. Han, Y. Matsui, N. Nagaosa, and Y. Tokura, Nature (London) **465**, 901 (2010).
[3] Y. Zheng and W. J. Chen, Rep. Prog. Phys. **80**, 086501 (2017).
[4] N. Nagaosa and Y. Tokura, Nat. Nanotechnol. **8**, 899 (2013).

[5] A. Fert, V. Cros, and J. Sampaio, Nat. Nanotechnol. **8**, 152 (2013).
[6] X. Z. Yu, N. Kanazawa, W. Z. Zhang, T. Nagai, T. Hara, K. Kimoto, Y. Matsui, Y. Onose, and Y. Tokura, Nat. Commun. **3**, 988 (2012).
[7] A. Casiraghi, H. Corte-León, M. Vafaee, F. Garcia-Sanchez, G. Durin, M. Pasquale, G. Jakob, M. Kläui, and O. Kazakova, Commun. Phys. **2**, 145 (2019).
[8] W. Chen, L. Liu, Y. Ji, and Y. Zheng, Phys. Rev. B **99**, 064431 (2019).
[9] A. Fert, N. Reyren, and V. Cros, Nat. Rev. Mater. **2**, 17031 (2017).
[10] K. Everschor-Sitte, J. Masell, R. M. Reeve, and M. Kläui, J. Appl. Phys. **124**, 240901 (2018).
[11] S. Mühlbauer, B. Binz, F. Jonietz, C. Pfleiderer, A. Rosch, A. Neubauer, R. Georgii, and P. Böni, Science **323**, 915 (2009).
[12] I. Lima Fernandes, J. Bouaziz, S. Blügel, and S. Lounis, Nat. Commun. **9**, 4395 (2018).
[13] J. Iwasaki, M. Mochizuki, and N. Nagaosa, Nat. Commun. **4**, 1463 (2013).
[14] A. A. Thiele, Phys. Rev. Lett. **30**, 230 (1973).
[15] K. Litzius, I. Lemesh, B. Krüger, P. Bassirian, L. Caretta, K. Richter, F. Büttner, K. Sato, O. A. Tretiakov, J. Förster, R. M. Reeve, M. Weigand, I. Bykova, H. Stoll, G. Schütz, G. S. D. Beach, and M. Kläui, Nat. Phys. **13**, 170 (2017).
[16] W. Jiang, X. Zhang, G. Yu, W. Zhang, X. Wang, M. Jungfleisch, J. Pearson, X. Cheng, O. Heinonen, K. L. Wang, Y. Zhou, A. Hoffmann, and S. G. E. te Velthuis, Nat. Phys. **13**, 162 (2017).
[17] R. Juge *et al.*, Phys. Rev. Appl. **12**, 044007 (2019).
[18] K. Litzius, J. Leliaert, P. Bassirian, D. Rodrigues, S. Kromin, I. Lemesh, J. Zazvorka, K.-J. Lee, J. Mulkers, N. Kerber, D. Heinze, N. Keil, R. M. Reeve, M. Weigand, B. Van Waeyenberge, G. Schütz, K. Everschor-Sitte, G. S. D. Beach, and M. Kläui, Nat. Electron. **3**, 30 (2020).
[19] U. Ritzmann, S. von Malottki, J.-V. Kim, S. Heinze, J. Sinova, and B. Dupé, Nat. Electron. **1**, 451 (2018).
[20] F. S. Yasin, J. Masell, K. Karube, A. Kikkawa, Y. Taguchi, Y. Tokura, and X. Yu, Proc. Natl. Acad. Sci. U.S.A. **119**, e2200958119 (2022).
[21] C. Reichhardt, C. J. O. Reichhardt, and M. V. Milosevic, Rev. Mod. Phys. **94**, 035005 (2022).
[22] R. Gruber, J. Zázvorka, M. A. Brems, D. R. Rodrigues, T. Dohi, N. Kerber, B. Seng, M. Vafaee, K. Everschor-Sitte, P. Virnau, and Mathias Kläui, Nat. Commun. **13**, 3144 (2022).
[23] K. Wang, Y. Zhang, V. Bheemarasetty, S. Zhou, S.-C. Ying, and G. Xiao, Nat. Commun. **13**, 722 (2022).
[24] F. Büttner, C. Moutafis, M. Schneider, B. Krüger, C. M. Günther, J. Gellhufe, C. v. Korff Schmising, J. Mohanty, B. Pfau, S. Schaffert, A. Bisig, M. Foerster, T. Schulz, C. A. F. Vaz, J. H. Franken, H. J. M. Swagten, M. Kläui, and S. Eisebitt, Nat. Phys. **11**, 225 (2015).
[25] L. Liu, W. Chen, and Y. Zheng, Phys. Rev. Lett. **128**, 257201 (2022).
[26] P. E. Roy, R. M. Otxoa, and C. Moutafis, Phys. Rev. B **99**, 094405 (2019).
[27] D. Pinna, G. Bourianoff, and K. Everschor-Sitte, Phys. Rev. Appl. **14**, 054020 (2020).
[28] A. P. Malozemoff and J. C. Slonczewski, *Magnetic Domain Walls in Bubble Materials*, edited by R. Wolfe (Academic Press, New York, 1979).
[29] W. Döring, Z. Naturforsch. **3**, 373 (1948).
[30] N. L. Schryer and L. R. Walker, J. Appl. Phys. **45**, 5406 (1974).
[31] O. A. Tretiakov, D. Clarke, G.-W. Chern, Y. B. Bazaliy, and O. Tchernyshyov, Phys. Rev. Lett. **100**, 127204 (2008).
[32] J. P. Zagorodny, Y. Gaididei, D. D. Sheka, J. G. Caputo, and F. G. Mertens, Phys. Rev. Lett. **93**, 167201 (2004).
[33] V. P. Kravchuk, D. D. Sheka, U. K. Rößler, J. van den Brink, and Y. Gaididei, Phys. Rev. B **97**, 064403 (2018).
[34] H. J. Schnitzer, F. G. Mertens, and A. R. Bishop, Physica (Amsterdam) **141D**, 261 (2000).
[35] V. P. Kravchuk, J. Magn. Magn. Mater. **367**, 9 (2014).
[36] F. G. Mertens, F. Cooper, S. Shao, N. R. Quintero, A. Saxena, and A. R. Bishop, J. Phys. A **50**, 145201 (2017).
[37] I. Dzyaloshinsky, J. Phys. Chem. Solids **4**, 241 (1958).
[38] T. Moriya, Phys. Rev. **120**, 91 (1960).
[39] See Supplemental Material at http://link.aps.org/supplemental/10.1103/PhysRevLett.131.246701 for simulation model and details (Sec. S1); derivation of the balance equation of generalized forces (Sec. S2); analytical form of the generalized forces (Sec. S3); Poisson's ratio and flexibility of the skyrmion (Sec. S4); deformation of skyrmions interacted with different defects (Sec. S5); motion of the skyrmion interacted with line defects (Sec. S6); motion of skyrmions interacted with point defects (Sec. S7); which includes Refs. [14,16,18,26,31,35,40–47].
[40] X. S. Wang, H. Y. Yuan, and X. R. Wang, Commun. Phys. **1**, 31 (2018).
[41] L. Liu, W. Chen, and Y. Zheng, Phys. Rev. Appl. **14**, 024077 (2020).
[42] M. Seemann, D. Ködderitzsch, S. Wimmer, and H. Ebert, Phys. Rev. B **92**, 155138 (2015).
[43] M. J. Donahue and D. G. Porter, OOMMF user's guide, version 1.0. NISTIR 6376 (1999).
[44] S. Rohart and A. Thiaville, Phys. Rev. B **88**, 184422 (2013).
[45] C. Reichhardt, D. Ray, and C. J. Olson Reichhardt, Phys. Rev. Lett. **114**, 217202 (2015).
[46] S. Kang, H. Kwon, and C. Won, J. Appl. Phys. **121**, 203902 (2017).
[47] Y. Hu, X. Lan, and B. Wang, Phys. Rev. B **99**, 214412 (2019).
[48] J. Iwasaki, W. Koshibae, and N. Nagaosa, Nano Lett. **14**, 4432 (2014).
[49] X. Zhang, G. P. Zhao, H. Fangohr, J. P. Liu, W. X. Xia, J. Xia, and F. J. Morvan, Sci. Rep. **5**, 7643 (2015).
[50] P. Lai, G. P. Zhao, H. Tang, N. Ran, S. Q. Wu, J. Xia, X. Zhang, and Y. Zhou, Sci. Rep. **7**, 45330 (2017).
[51] J. Castell-Queralt, L. González-Gómez, N. Del-Valle, A. Sanchez, and C. Navau, Nanoscale **11**, 12589 (2019).
[52] I. Purnama, W. L. Gan, D. W. Wong, and W. S. Lew, Sci. Rep. **5**, 10620 (2015).